ELSEVIER

Journal of Power Sources 112 (2002) 90–97

JOURNAL OF POWER SOURCES

www.elsevier.com/locate/jpowsour

Electrochemical characteristics of tubular flat-plate-SOFCs fabricated by co-firing cathode substrate and electrolyte

Himeko Orui*, Kimitaka Watanabe, Masayasu Arakawa

NTT Telecommunications Energy Laboratories, 31 Morinosato-Wakamiya, Atsugi-shi, Kanagawa 243-0198, Japan

Received 21 February 2002; received in revised form 27 May 2002; accepted 10 June 2002

Abstract

Tubular flat-plate (TFP)-solid oxide fuel cells (SOFCs) supported by cathodes with gas flow channels were fabricated by co-firing the cathodes and electrolytes. The size of a single cell is 43 mm × 4.5 mm × 100 mm, and the maximum power density of 0.83 W/cm^2 was achieved at a current density of 1.6 A/cm^2 at 1000 °C. We studied the electrochemical characteristics of the anode and the cathode by the ac impedance method. The resistance corresponding to the reaction around the three-phase boundaries of the anode/electrolyte interface increases with decreasing temperature from 1000 to 800 °C in the Ni–Y_2O_3 stabilized ZrO_2 (YSZ) anode of the TFP cell. From ac impedance measurements made at various oxygen partial pressures P_{O_2}, we found that under high P_{O_2} ($\log P_{O_2} > -0.77$) surface diffusion of adsorbed oxygen atoms was the dominant step, but under low P_{O_2} ($\log P_{O_2} < -0.77$) the diffusion of oxygen gas was the rate-determining step in the cathode reaction in this TFP cell.

Keywords: Solid oxide fuel cell; Co-firing; Tubular flat-plate type cell; Cathode substrate; Oxygen partial pressure; Cell performance

1. Introduction

The solid oxide fuel cell (SOFC) is a promising power generation system because of potential for high energy-conversion efficiency and low environmental pollution. Since SOFCs are made from brittle ceramic materials, cell design is important not only for the cell performance but also for the stacking strength. The SOFC structure is mainly tubular or planar. Tubular-type cells have a high strength for stacking and easy handling for gas sealing. Making the most of these advantages, Siemence Westinghouse has developed a 220 kWe pressurized SOFC/gas turbine combined power plant [1]. For the commercialization of SOFC systems, it is necessary to reduce the cost of fabricating high-performance cell stacks. But the fabrication process of tubular cells is complicated and sometimes requires expensive apparatuses, such as an EVD. In addition, cell performance is limited by the long current path in the circumferential direction. On the other hand, planar-type SOFCs are expected to offer high power density because their shorter current path results in low ohmic resistance. Conventional SOFCs are usually operated at 1000 °C, but if this could be reduced below 850 °C, metal alloys could be used for the interconnection, which would reduce cost. Many recent planar-type cells are anode-supported and basically consist of a 1–2 mm thick anode and 5–15 μm thick electrolyte. Such anode-supported cells, even though consisting of conventional materials, show high power density above 0.6 W/cm^2 at 800 °C [2]. However, gas separation, sealing, and stacking stress are still problems when planar-type cells are stacked.

We have designed a tubular flat-plate (TFP) structure and have reported of high-performance [3]. In TFP-type SOFCs, a higher power density is expected, because resistance is reduced due to having a shorter current path length compared to tubular-type SOFCs [4]. In addition TFP-type SOFCs can be assembled into stacks more easily than planer SOFCs. We have also proposed a cathode-supported type that enables us to use nickel material for electrical connection of the cells [5].

Co-firing is suitable for making low-cost, high-performance cells, because it is a simple process and a thin electrolyte can be formed. There have been only a few reports on the characteristics of the cells made by co-firing of the cathodes and the electrolytes because of the fabrication difficulties. We have successfully fabricated small cathode-supported planar cells by co-firing [6]. In this report, we describe fabrication of a TFP cell by co-firing of the cathode and the electrolyte, and discuss the single-cell performance and electrochemical characteristics of the TFP cell.

* Corresponding author. Tel.: +81-46-240-2711; fax: +81-46-270-2702.
E-mail address: himeko@aecl.ntt.co.jp (H. Orui).

0378-7753/02/$ – see front matter
PII: S0378-7753(02)00346-4

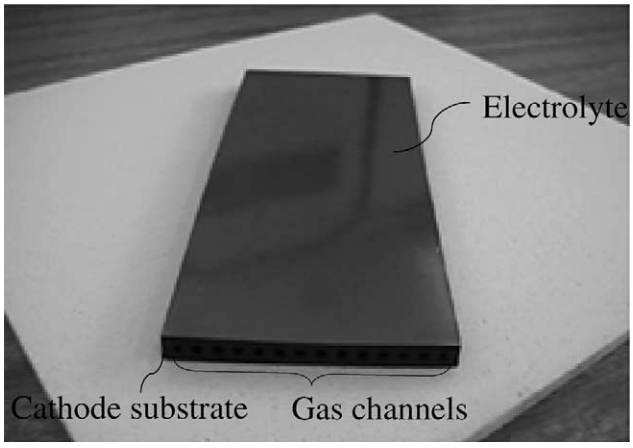

Fig. 1. TFP cell fabricated by co-firing a cathode substrate and an electrolyte.

2. Experimental

The 8 mol% Y_2O_3 stabilized ZrO_2 (YSZ; Tosoh) was used for the electrolyte. A mixture of 70 wt.% $La_{0.7}Sr_{0.3}MnO_3$ (LSM; Seimi Chemical) and 30 wt.% YSZ was used for the cathode. Ceramic sheets of electrolytes and cathodes were prepared by the doctor blade method. In order to control the porosity of the cathode, spherical carbon powder was added to the cathode powder as a poresizer [6]. The porosity of sintered cathode was estimated as the ratio of the measured density of the sintered body to the theoretical density of cathodes [6].

Gas permeability coefficient K was calculated as:

$$K\left(\frac{\text{ml cm}}{\text{g s}}\right) = \frac{Q\theta}{(A\Delta p)}$$

where Q is the amount of permeated gas, Δp the pressure difference across the specimen, A the measurement area, and θ is the sample thickness. Nitrogen gas was used for the gas permeability measurements.

The conductivity of the sintered cathode was measured by the four-terminal method at 1000 °C and the microstructure of the co-fired cell was observed by scanning electron microscopy (SEM).

The TFP cells were fabricated by the co-firing method. Ceramic sheets of cathode and an electrolyte were cut to an appropriate size, laminated, and co-fired at 1300 °C to make the cathode substrate with an electrolyte layer. Fig. 1 shows the configuration of a two-layer TFP half cell. The cell consists of an air electrode substrate with 14 gas channels, and a thin electrolyte. It is 100 mm long, 43 mm wide, and 4.5 mm thick.

Platinum pastes (Tokuriki Chemical) or cermets of 60 wt.% NiO (Furuuchi Chemical) and YSZ were used for the anode. Anode size was 6 or 18 cm^2. The calcination temperatures of platinum and NiO–YSZ were 1000 and 1300 °C, respectively. The platinum mesh was used as the current collector for the anode and the cathode. The current and voltage leads were connected to the current collector. Fig. 2 shows the structure of the cell holder for the electrochemical measurements. Both the top and the bottom of the cell were sealed with glass to make the system gastight. Hydrogen was the fuel and oxygen was the oxidant. The flow rate of both gases was 1 l/min. TFP cell performance was measured by a dc polarization method at 1000 and 800 °C. The electrochemical characteristics were evaluated by an ac impedance method around the open circuit voltage.

To study the influence of gas composition on the electrochemical characteristics of the cell, we cut disks about 3 cm in diameter from the TFP cell. The current–voltage (I–V)

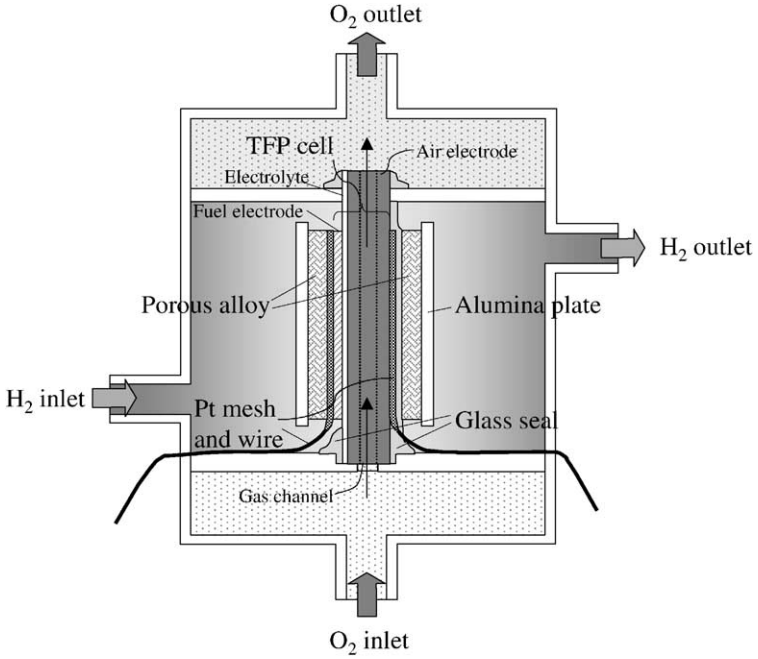

Fig. 2. Schematic diagram of the apparatus for the power generation experiment.

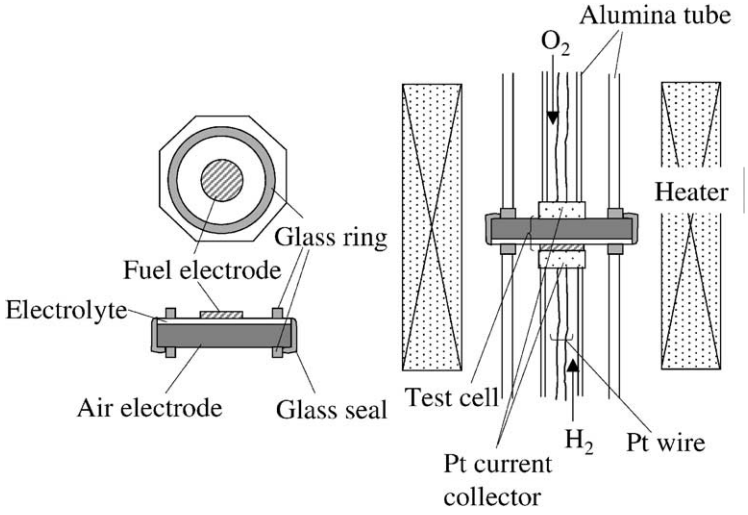

Fig. 3. Schematic diagrams of the test cell fixed in the apparatus for the power generation test.

characteristics and ac impedance spectra of those small cells were measured at 1000 °C. Fig. 3 shows the test cell structure and the apparatus for the power generation experiment. The NiO–YSZ cermets were screen-printed on the electrolyte as an anode and sintered with platinum mesh used as the current collector. The fuel was either pure hydrogen or humidified hydrogen with water content of several percents. The oxidant was a mixture of oxygen and nitrogen. The partial pressure was controlled by varying the oxygen–nitrogen ratio. The flow rate of fuel and oxidant gases was either 0.5 or 0.1 l/min.

3. Results and discussion

3.1. Physical characteristics of co-fired cells

Since the air electrode occupies most of the space in our TFP cell, its electrical and physical characteristics will greatly affect the power generation characteristics of the cell. Fig. 4 shows the gas permeability coefficient and electrical conductivity dependence on the porosity of the air electrode. In general, there is a trade-off relationship between gas permeability and electrical conductivity. Ohashi et al. reported that if the cathode gas permeability was 10^{-3} to 10^{-4} ml cm/(g s), sufficient oxygen was supplied at 0.5–1 A/cm^2 for the cathode-supported cells [7]. In this work, the porosity was adjusted to be around 30%, where the gas permeability was over 10^{-4} ml cm/(g s).

Fig. 5 shows cross-sectional SEM images of the co-fired TFP half-cell consisting of an air electrode substrate and a thin electrolyte. The thickness of the electrolyte was approximately 20 μm and the adhesion between the substrate and the electrolyte was quite good. The physical characteristics of the co-fired half-cell are summarized in Table 1. The porosity of this cathode was 33% and that of the electrolyte was <3%. The cathode had sufficient gas permeability of 1.31×10^{-4} ml cm/(g s), but the electrical conductivity was slightly low because the cathode was made from a mixture of LSM and YSZ. No gas permeability was detected for the co-fired cathode and electrolyte, which indicated that the electrolyte was dense enough for practical use.

3.2. Electrochemical characteristics of TFP cells

Fig. 6 shows the *I–V* characteristics of the TFP-type cell with an platinum anode of 6 cm^2 at 1000 °C for various hydrogen flow rates. The *I–V* characteristics for the hydrogen flow rates of 1 and 2 l/min are almost the same, but for 0.5 l/min there is a large voltage drop against the current density. Fig. 7 shows the voltage change of this TFP cell against the hydrogen flow rate at a current density of 0.7 A/cm^2. There is a large voltage drop for the hydrogen

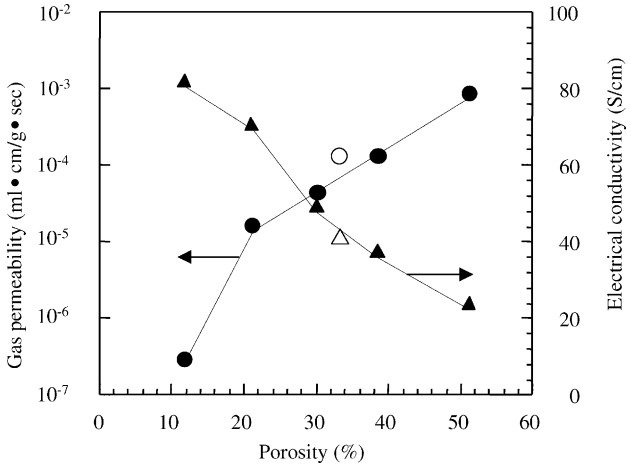

Fig. 4. Effect of porosity of air electrode on gas permeability and electrical conductivity. The white marks indicate the values for the sintered LSM actually used.

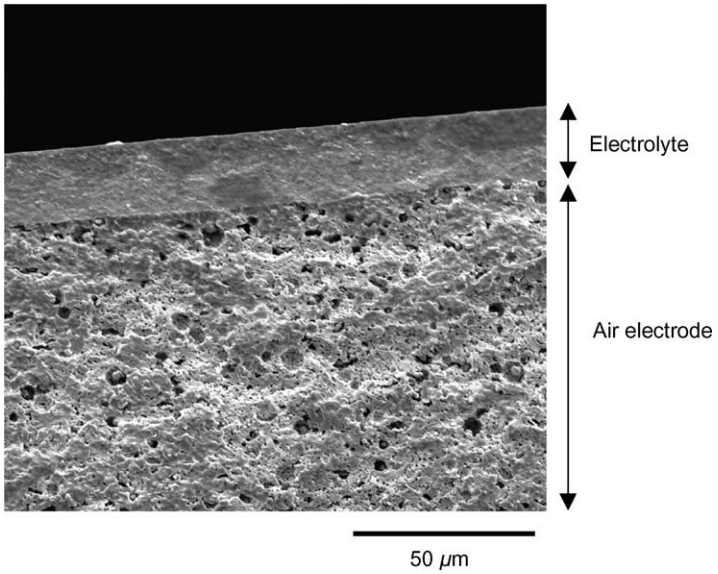

Fig. 5. Cross-sectional SEM image of the co-fired cathode and electrolyte.

Table 1
Physical characteristics of the electrolytes and the air electrodes

	Material	Electrical conductivity (S/cm)	Porosity (%)	N_2 gas permeability (ml cm/(g s))
Electrolyte	8-YSZ	0.1	3.0	–
Air electrode	$La_{0.7}Sr_{0.3}MnO_3$ + 30wt.% YSZ	39.2	33.7	1.3×10^{-4}

flow rate below 0.8 l/min, but the voltage remains constant at flow rates above 1 l/min. From this result, we decided to perform the measurements of the power generation characteristics for TFP cells at the hydrogen flow rate of 1 l/min. The fuel utilization was 2.9% at 0.7 A/cm^2. Such a low fuel utilization might be caused by the fact that a large amount of fuel was lost before it arrived at the anode reaction area by gas leakage at the seal part of the cell holder.

Fig. 8 shows the *I–V* characteristics of the TFP cell with Ni–YSZ anode of 18 cm^2 at 1000 and 800 °C. A maximum power density of 0.83 W/cm^2 at a current density of 1.6 A/cm^2 was obtained at 1000 °C. But when the temperature

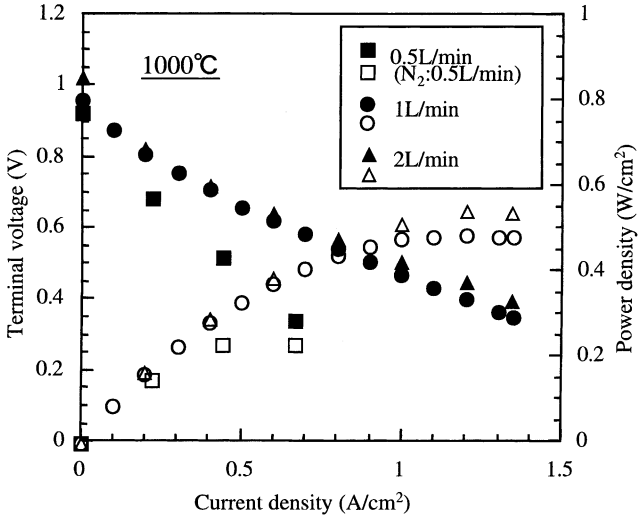

Fig. 6. Power generation characteristics of the co-fired TFP cell with the Pt anode at 1000 °C. O_2 and H_2 were the oxidant and the fuel, respectively.

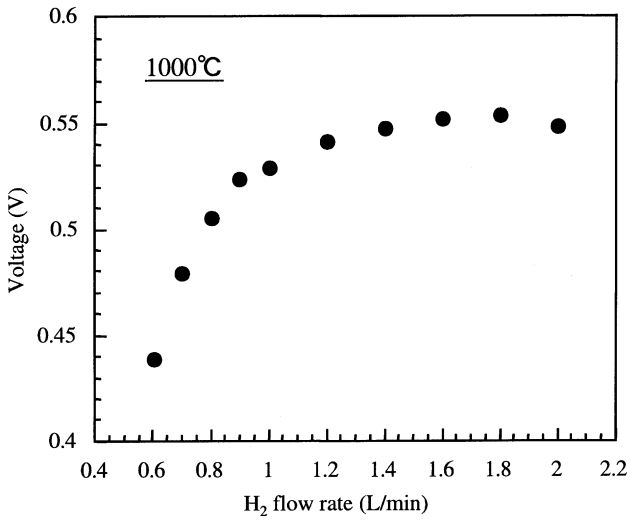

Fig. 7. H_2 flow rate dependence on the voltage of the TFP cell with the Pt anode at 0.7 A/cm^2. The flow rate of O_2 gas was 1 l/min.

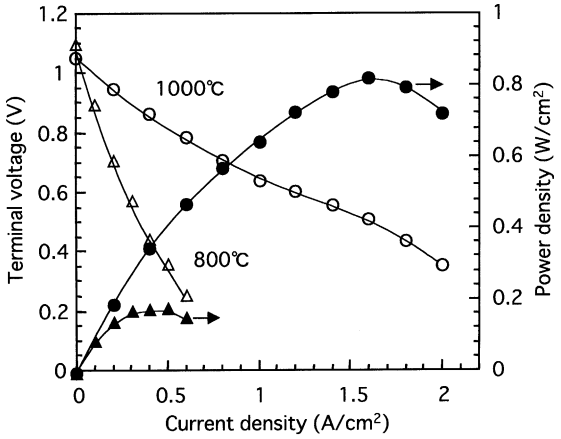

Fig. 8. Power generation characteristics of the co-fired TFP cell with the Ni–YSZ anode. O_2 and H_2 were the oxidant and the fuel, respectively. The flow rate of each gas was 1 l/min.

decreased to 800 °C, the overvoltage increased and maximum power density decreased to 0.18 W/cm^2. This implies that the internal resistance of this cell largely depends on the operating temperature.

To study the electrochemical characteristics of this TFP cell in detail, we measured ac impedance spectra of the TFP cell. We measured the impedance between the anode and the cathode, because the working and counter electrodes are not symmetrical in the TFP cell and we can use no reference electrode [8]. The ac impedance spectra of the TFP cell with a Pt or Ni–YSZ anode of 18 cm^2 at 1000 or 800 °C are shown in Fig. 9(a)–(c). The spectra contain two or three arcs, and we obtained R_0 and R_1-R_3. R_0 is the intersection point to the real part in the high-frequency range, and R_1-R_3 are obtained from the diameter of the arcs (C_1-C_3) which appear in each frequency range: C_1 appears above several hundred Hz, C_2 between 10 and several hundred Hz, and C_3 below 10 Hz. The R values are summarized in Table 2 which also includes the values estimated from ac impedance spectra of a small test cell under the different P_{O_2} conditions. These data reveal the bulk resistance (R_0) to be 10 times larger than the value calculated from the material resistance. Roosmalen and Cordfunke studied the reactivity between $La_{1-x}Sr_xMnO_3$ ($x = 0$–0.5) and YSZ, and reported that $La_{0.7}Sr_{0.3}MnO_3$ seems to be the best candidate for a long-term operation at 1000 °C, but highly-resistive pyrochlores of $La_2Zr_2O_7$ and/or $SrZrO_3$ are formed up to 1000 °C [9]. Though we have not yet confirmed it, one possible reason for the high bulk resistance in the ac impedance spectra is that a highly-resistive pyrochlore layer might form between the cathode and the electrolyte at 1300 °C during the co-firing process.

At 1000 °C, R_1 of the TFP cell with the Pt anode is larger than that of the cell with the Ni–YSZ anode, though R_3 of both cells is almost the same. The Ni–YSZ cermet anode might have a larger three-phase boundary length than the simple metal electrode. Therefore, R_1 is considered to be the reaction resistance which depends on the anode microstructure. Mogensen et al. also found two or three arcs in the ac impedance spectra of the Ni–YSZ anode [10]. They explained that the high-frequency arc reflects the resistance of proton transfer from the Ni surface to the YSZ surface, which should be inversely proportional to the three-phase boundary length. On the other hand, R_3 shown in Table 2 is considered to be the resistance for cathode reactions, for which R_3 increases with decreasing oxygen partial pressure.

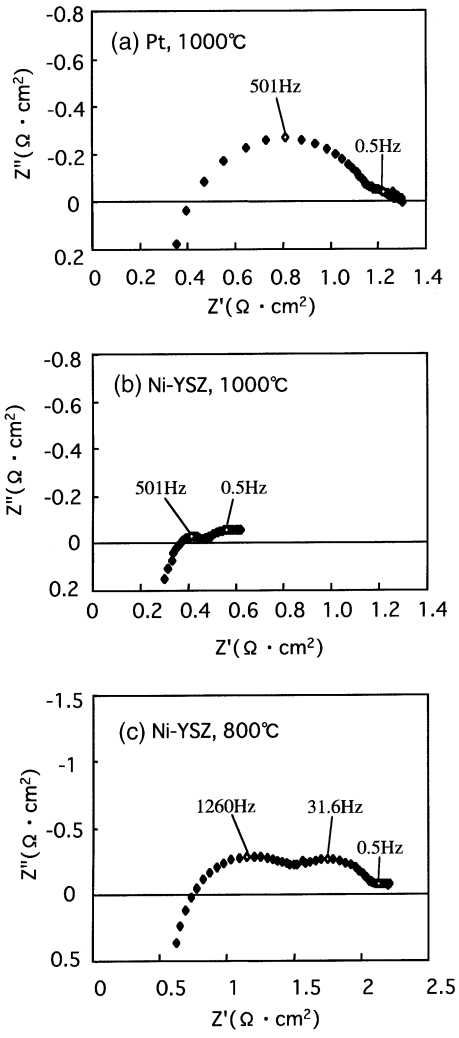

Fig. 9. The ac impedance spectra of co-fired TFP cells.

Table 2
Resistances estimated from the ac impedance spectra

	Resistance (Ω cm^2)			
	R_0	R_1	R_2	R_3
Pt, 1000 °C	0.41	0.76	–	0.15
Ni–YSZ, 1000 °C	0.37	0.12	–	0.18
Ni–YSZ, 800 °C	0.75	0.97	0.78	0.21
Ni–YSZ, P_{O_2}: 1 atm[a]	0.46	0.20	–	0.13
Ni–YSZ, P_{O_2}: 0.17 atm[a]	0.47	0.20	–	0.32

[a] Values estimated from the ac impedance spectra of a small test cell at 1000 °C.

Our results also show that R_1 increases and R_2 appears with decreasing temperature from 1000 to 800 °C. The increase in R_1 at 800 °C implies that the resistance of proton transfer around the three-phase boundary strongly depends on the operating temperature in this Ni–YSZ anode reaction. R_2 is not yet identified; we need more investigation to reveal the origin of this resistance component.

3.3. Electrochemical characteristics of small cells

In order to study the electrochemical characteristics of each electrode, we use small test cells to easily control the partial pressure of each gas.

The *I–V* characteristics for a gas flow rate of 0.5 l/min with pure and humidified hydrogen are shown in Fig. 10. Water vapor was supplied by a water bubbler at room temperature, and we estimated the P_{H_2O} from OCV via the Nernst equation:

$$E = E_0 + \frac{RT}{nF} \ln\left(\frac{P_{H_2} P_{O_2}^{1/2}}{P_{H_2O}}\right)$$

The open circuit voltage was 1.2 V for pure hydrogen and 1.1 V for humidified hydrogen, which corresponds to the water vapor concentration of 3%. The cell using humidified hydrogen exhibits higher power generation characteristics than the cell using pure hydrogen at a higher current density. This agrees with the results in [11,12]. Those reports suggest that the appropriate amount of water in the hydrogen can considerably reduce the interfacial resistance at the anode. The role of water in hydrogen oxidation is not clearly understood, but it has been suggested that the water adsorbs to YSZ electrolyte and broadens the reactive areas around the triple-contact point, thereby increasing the reaction rate [13].

The *I–V* characteristics for a gas flow rate of 0.1 l/min are shown in Fig. 11. The limiting current appears around 0.5 A/cm^2. This means that not enough gas was supplied to the cell reaction point above 0.5 A/cm^2 for this gas flow rate. When we use the humidified hydrogen for fuel, the open circuit voltage decreases from 1.2 to 1.05 V, which corresponds to 6% humidified hydrogen. However, the *I–V* curve above 0.2 A/cm^2 was almost the same as that for dry hydrogen.

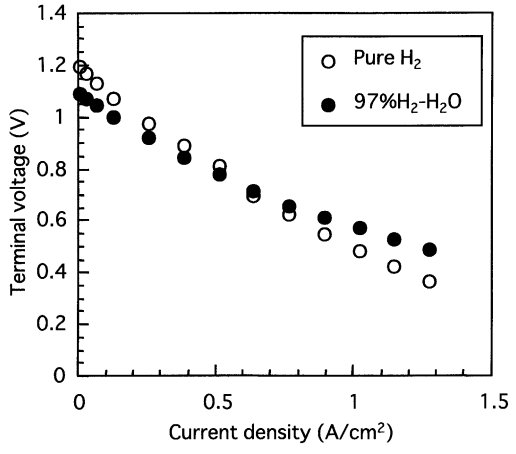

Fig. 10. *I–V* characteristics of the two-layer co-fired cell using pure H_2 or 97% H_2–H_2O as a fuel. The flow rate of each gas was 0.5 l/min.

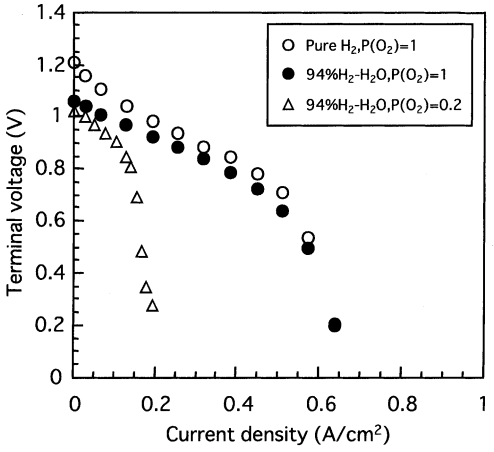

Fig. 11. *I–V* characteristics of the two-layer co-fired cell using pure H_2 or 97% H_2–H_2O as a fuel. The flow rate of each gas was 0.1 l/min.

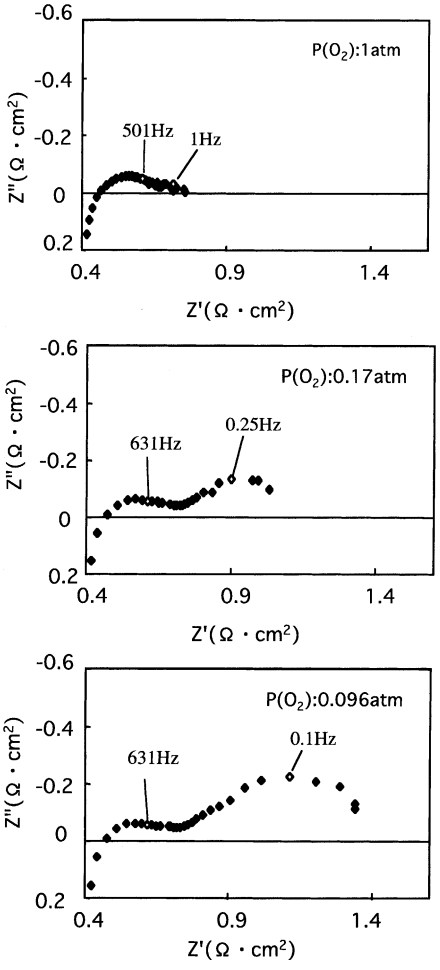

Fig. 12. The ac impedance spectra of co-fired test cell at 1000 °C.

This does not contradict the results in Fig. 10. The characteristics for pure oxygen and a mixture of oxygen and nitrogen that approximates the composition of air ($P_{O_2} = 0.2$) are also shown in Fig. 11. In the $P_{O_2} = 0.2$, the limiting current appears at 0.15 A/cm^2, whereas it appears at 0.5 A/cm^2 in the pure oxygen. This suggests that the power generation characteristics of this cell strongly depend on the oxygen diffusion through the air electrode.

In order to investigate the electrochemical characteristics of the cathode substrate, we measured the ac impedance for various partial pressures of oxygen. Some results for 1000 °C are shown in Fig. 12. The high-frequency arc does not depend very much on the partial pressure, but the diameter of low-frequency arc increases as the partial pressure decreases. Mizusaki et al. studied the relationship between the conductivity of the cathode interface, σ_E and partial pressures of oxygen P_{O_2} and explained the rate-determining step using the cathode reaction model [14]. In order to clarify the rate-determining step of this TFP cathode, we calculated the conductivity of the electrode interface, σ_E, using:

$$\sigma_E = \frac{1}{AR_E}$$

where A is the apparent electrode area and R_E is the resistance obtained from the low-frequency semicircle of the ac impedance spectra [15]. Fig. 13 shows the P_{O_2} dependence of σ_E measured at 1000 °C. When the partial pressure of oxygen is high ($\log P_{O_2} > -0.77$), σ_E is roughly proportional to the $P_{O_2}^{1/2}$. But for a low ($\log P_{O_2} < -0.77$), σ_E is directly proportional to the P_{O_2}. This means that, for a high partial pressure, the rate-determining step for the cathode reaction is the surface diffusion of adsorbed oxygen. But for a low partial pressure, the reaction rate is determined by the diffusion of oxygen gas [15]. The cathode in our cell is about 2 mm thick for a high mechanical strength. We cannot ignore the diffusion resistance of oxygen gas through the thick air electrode substrate. Tachibana et al. reported the relationship among the cathode thickness, porosity, and power generation characteristics for a cathode-supported tubular cells [16]. According to their results, in case that the cathode is thick and/or dense, the power density drastically decreases due to the slow gas diffusion through the cathode, especially when a low P_{O_2} oxidant gas such as air is used. As shown in Fig. 8, when the sufficient oxygen gas was supplied, the TFP cell showed satisfactory high power generation characteristics. In order to achieve a high power density with an electrode-supported cell, the thickness of supported electrode should be decreased as much as possible to avoid the influence of gas diffusion, and the gas flow condition through the supported electrode should be adjusted to ensure reactant gas transport to the three-phase boundaries.

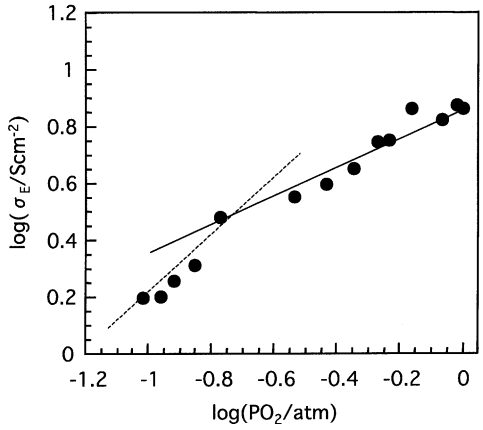

Fig. 13. The P_{O_2} dependence of σ_E at 1000 °C.

4. Conclusions

We have fabricated TFP cells by co-firing two layers: a porous air electrode and a dense 20 μm thick electrolyte. A cell with a Ni–YSZ anode exhibited a maximum power density of 0.83 W/cm^2 at 1000 °C. The small amount of water in the fuel gas decreased the overvoltage of the cell at high current densities when sufficient gas was supplied. The dependence of σ_E on the partial pressure of oxygen indicates that, for a high oxygen partial pressure, the reaction rate at the cathode is determined by the surface diffusion of adsorbed oxygen atoms. But when the partial pressure of oxygen is below ca. 0.16 atm, the reaction rate is determined by the diffusion of oxygen gas in the cathode. To further improve the cell performance, we need to ensure sufficient oxygen gas transport through the cathode substrate to the three-phase boundaries.

References

[1] S.E. Veyo, S.D. Vora, Abstracts of 2000 Fuel Cell Seminar, 2000, p. 477.
[2] J.P. Ouweltjes, F.P.F. van Berkel, P. Nammensma, G.M. Christie, in: S.C. Singhal, M. Dokiya (Eds.), Proceedings of the Electrochemical Society Series on Solid Oxide Fuel Cells VI, PV 99-19, Pennington, NJ, 1999, p. 803.
[3] T. Matsushima, D. Ikeda, H. Kanagawa, T. Hirai, A. Komura, Abstracts of 1996 Fuel Cell Seminar, 1996, p. 139.
[4] S.C. Singhal, in: S.C. Singhal, M. Dokiya (Eds.), Proceedings of the Electrochemical Society Series on Solid Oxide Fuel Cells VI, PV 99-19, Pennington, NJ, 1999, p. 39.
[5] M. Arakawa, K. Watanabe, H. Ohrui, K. Nozawa, Y. Tabata, T. Hirai, Abstracts of 2000 Fuel Cell Seminar, 2000, p. 603.
[6] H. Ohrui, T. Matsushima, T. Hirai, J. Power Sources 71 (1998) 185.
[7] R. Ohashi, F. Hayashi, O. Yamamoto, Denki Kagaku 62 (9) (1994) 797.
[8] D. Ikeda, H. Kanagawa, T. Matsushima, Denki Kagaku 64 (6) (1996) 629.
[9] J.A.M. van Roosmalen, E.H.P. Cordfunke, Solid State Ionics 52 (1992) 303.
[10] M. Mogensen, et al., in: Proceedings of the Electrochemical Society Series on Solid Oxide Fuel Cells IV, PV 95-1, Pennington, NJ, 1995, p. 657.

[11] D.W. Dees, U. Balachandran, S.E. Dorris, J.J. Heiberger, C.C. McPheeters, J.J. Picciolo, in: S.C. Singhal (Ed.), Proceedings of the First International Symposium on Solid Oxide Fuel Cells, Electrochemical Society Proceedings Series, PV 89-11, Pennington, NJ, 1989, p. 317.
[12] F.Z. Mohamedi-Boulenouar, J. Guindet, A. Hammou, in: U. Stimming, S.C. Singhal, H. Tagawa, W. Lehnert (Eds.), Proceedings of the Electrochemical Society Series on Solid Oxide Fuel Cells, PV 97-18, Pennington, NJ, 1997, p. 441.
[13] N.Q. Minh, T. Takahashi, Science and Technology of Ceramic Fuel Cells, Elsevier, Amsterdam, 1995, p. 204.
[14] J. Mizusaki, K. Amano, S. Yamauchi, K. Fueki, Solid State Ionics 22 (4) (1987) 313.
[15] H. Kamata, A. Hosaka, J. Mizusaki, H. Tagawa, Solid State Ionics 106 (1998) 237.
[16] K. Tachibana, H. Nakashima, A. Sakamoto, A. Ueno, M. Kuroishi, M. Aizawa, K. Eguchi, H. Arai, Abstracts of 1994 Fuel Cell Seminar, 1994, p. 511.